Senescent Dermal Fibroblasts Decrease Stemness in Basal Keratinocytes in a Bioengineered Model of Human Full-Thickness Skin

JID Open

Journal of Investigative Dermatology (2024) ■, ■–■; doi:10.1016/j.jid.2024.07.004

TO THE EDITOR

Intrinsic skin aging is characterized by decreased regenerative capacity and impaired differentiation of epidermal keratinocytes (KCs), resulting in a thinning of the epidermis, which contributes to a compromised barrier function. Cell senescence is a hallmark of aging, and senescent fibroblasts, KCs, melanocytes, and others accumulate in aging skin (Low et al, 2021). Accumulation of senescent dermal fibroblasts has been widely hypothesized as a cause of dermal and epidermal aging. This is because senescent cells secrete a wide range of bioactive molecules termed the senescence-associated secretory phenotype, which induce aging-like bystander effects in neighboring cells and tissues and because aging could be postponed by anti-senescence interventions in many organs (Kirkland and Tchkonia, 2017). However, the specific evidence for senescent fibroblasts causing epidermal aging is still not strong (Low et al, 2021).

Bioengineered skin equivalents capture the complexity of human skin in vitro and enable interactions between different cell populations to be studied. A small number of 3-dimensional skin equivalents have been developed that test the impact of senescent dermal fibroblasts (Diekmann et al, 2016; Janson et al, 2013; Weinmüllner et al, 2020). Results were not unequivocal: in a collagen-based matrix, senescent fibroblasts induced hallmarks of intrinsic skin aging, including epidermal thinning, reduction of basal KC proliferation, impairment of epidermal differentiation, and loss of barrier function (Weinmüllner et al, 2020). In a collagen–glycosaminoglycan–chitosan scaffold, senescent fibroblasts reduced epidermal FLG as well as dermal collagen and elastin expression but had no effect on epidermal thickness (Diekmann et al, 2016). Finally, in a fibroblast-derived matrix in a polyester permeable support (Janson et al, 2013), late population doubling (senescent) fibroblasts caused a thinner dermis and minor changes in the epidermal expression of keratins 6 and 10 but no changes in epidermal thickness, KC proliferation, or basement membrane formation.

A main limitation of previous skin equivalents is variability due to the use of complex protocols and of exogenous extracellular matrix proteins. We recently developed a robust full-thickness skin equivalent that is highly reproducible owing to the use of an inert porous polystyrene membrane (Alvetex) as scaffold, commercially available cells, and defined low-serum media. The scaffold allows human dermal fibroblasts to produce their own endogenous extracellular matrix proteins, which alleviates the need for exogenous collagen and fully supports the differentiation and stratification of the epidermis (Costello et al, 2019; Roger et al, 2019). In this study, we bioengineered Alvetex-based human full-thickness skin models containing variable fractions of senescent fibroblasts (from 0 to 100% seeding density [Supplementary Figure S1 provides the details]). Dermal equivalents were matured for 28 days followed by formation of an epidermal layer for 14 days (details are provided in Supplementary Materials and Methods). Four independent experiments were performed varying the senescent fibroblast seeding density between 0 and 20% (experiments 1–3) or between 0 and 100% (experiment 4). Models from every experiment were divided in 2, and technical repeats (including independent sectioning, staining, imaging, and quantification) were done in separate laboratories, with laboratory B being fully blinded to the fraction of senescent fibroblasts in the sample.

Incorporation of senescent fibroblasts in the dermal component induced senescence-associated secretory phenotype components already at 20% seeding density (Supplementary Figure S2). Accordingly, there was a decrease of total collagen in the skin equivalents created with higher senescent human dermal fibroblast frequencies (Supplementary Figure S3). Epidermal thinning with increased senescent cell load (Supplementary Figure S4) was significant, with $P < .05$ (Figure 1a). Qualitatively, there was no evidence for changed epidermal differentiation as judged by costaining for cytokeratins 10 and 14 (Supplementary Figure S5). To test whether senescent dermal fibroblasts induce senescence in basal KCs, we measured cell and nuclear size and Ki-67 and HMGB1 expressions (also in suprabasal cells). There were no changes in basal KC size (Figure 1b), basal KC nuclear size (Figure 1c), or HMGB1 positivity of either basal (Figure 1d and Supplementary Figure S6a) or suprabasal (Figure 1g) KCs, and there was even an increase in Ki-67–positive KCs with increasing load of senescent fibroblasts (Figure 1e and Supplementary Figure S6c). However, lower frequencies of basal KCs were positive for the epithelial stemness marker p63 under high senescence loads (Figure 1f and Supplementary Figure S6b). In contrast, frequencies of p63-positive KCs in the suprabasal

Abbreviation: KC, keratinocyte

Accepted manuscript published online XXX; corrected proof published online XXX

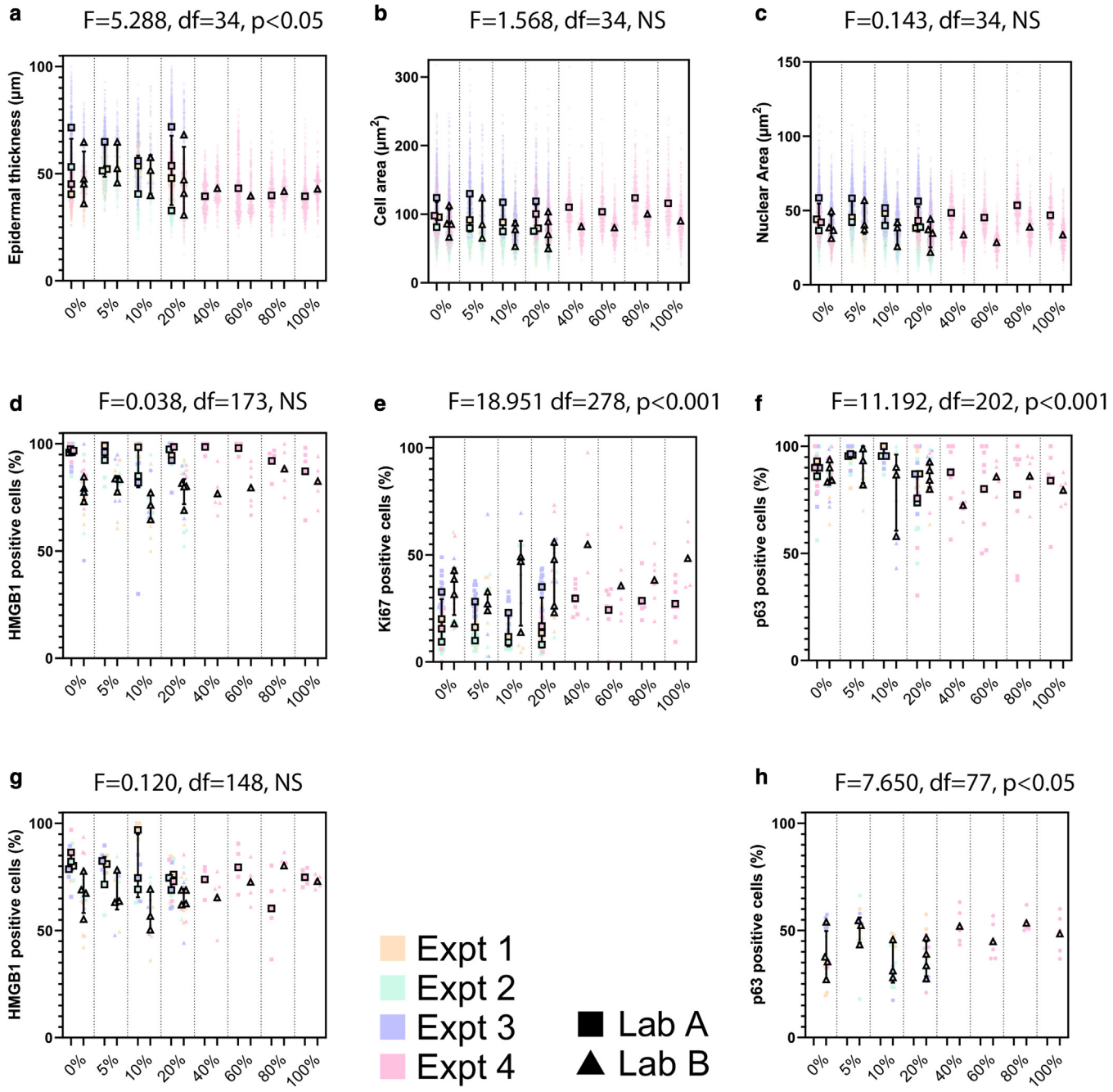

Figure 1. Effects of increasing frequencies of senescent dermal fibroblasts onto the epidermal compartment. Four separate experiments were performed, constructing skin models with variable amounts of senescent dermal fibroblasts (senescent cell seeding densities between 0 and 20% for experiments 1−3 and between 0 and 100% for experiment 4). Technical repeats were performed in independent laboratories, with laboratory B being fully blinded. (**a**) Epidermal thickness, (**b**) basal cell area, (**c**) basal cell nuclear area, (**d**) fractions of HMGB1-positive basal cells, (**e**) fractions of Ki-67−positive basal cells, (**f**) fractions of p63-positive basal cells, (**g**) fractions of HMGB1-positive suprabasal cells, and (**h**) fractions of p63-positive suprabasal cells. F-test results were calculated by linear regression. F-test values (F), degrees of freedom (denoted as df), and significance for the regression slope (p) are indicated. NS, not significant.

layer increased with senescent load (Figure 1h).

A 2-way ANOVA on the untransformed data revealed a systematic observer bias for most parameters (Supplementary Table S1). However, when the same analysis was performed on the normalized data, observer effects were mostly canceled out (Supplementary Table S2). This suggested variation between experiments as the main variation source, whereas intraexperimental and interobserver factors resulted in a bias in absolute values but not in the ability to detect experimentally induced differences. Specifically, results appeared not dependent on observer blinding.

In conclusion, although senescent fibroblasts induced a senescence-associated secretory phenotype similar to observations in aged skin (Low et al, 2021) and in collagen-based 3-dimensional skin models (Weinmüllner et al, 2020), they did not induce KC senescence. However, they did cause a reduction of the stemness

marker p63, specifically in the basal layer, which might be the cause of the observed epidermal thinning. Matrix composition may be a major modifier of the effect of senescent fibroblasts onto the epidermal equivalent. Aging-like epidermal changes were reported in collagen-based skin models containing senescent fibroblasts (Weinmüllner et al, 2020) but not in a skin model using polyester-based material (Janson et al, 2013). It is well-known that cellular senescence not only reshapes the matrix (Mavrogonatou et al, 2023), but extracellular matrix properties also significantly impact on the senescent cell phenotype, including senescence-associated secretory phenotype intensity and composition (Blokland et al, 2020).

Taken together, our data reveal the context and probably matrix dependency of the effects of senescent fibroblasts in human full-thickness skin equivalents. Senescent fibroblasts may drive skin intrinsic aging by different mechanisms depending on their environment, suggesting that besides interventions that reduce cell senescence, there may also be others, specifically those impacting on the extracellular matrix that might have potential to reduce skin aging.

ETHICS STATEMENT

This study was performed in accordance with the Declaration of Helsinki. No human or animal experiments were performed in this study.

DATA AVAILABILITY STATEMENT

Datasets related to this article can be found at https://data.mendeley.com/datasets/w8d49vjnkt/1, an open-source online data repository hosted at Mendeley Data.

KEYWORDS

Aging; Artificial skin; Fibroblasts; Keratinocytes; Senescence

ORCIDs

Evon Low: http://orcid.org/0000-0002-4978-5123
Lucy A. Smith: http://orcid.org/0000-0002-7142-4471
Satomi Miwa: http://orcid.org/0000-0002-1239-1198
Edward Fielder: http://orcid.org/0000-0003-2834-8706
Stefan Przyborski: http://orcid.org/0000-0001-7613-525X
Thomas von Zglinicki: http://orcid.org/0000-0002-5939-0248

CONFLICT OF INTEREST

SP acts as a technical consultant with the company Reprocell Europe. Proctor&Gamble cofunded part of the Biotechnology and Biological Sciences Research Council grant number BB/S006710/1 to TvZ. The remaining authors state no conflict of interest.

ACKNOWLEDGMENTS

The authors acknowledge funding by Biotechnology and Biological Sciences Research Council/P&G (number BB/S006710/1) and H2020 WIDESPREAD (project 857524) to TvZ and Biotechnology and Biological Sciences Research Council (number BB/S007431/1) to SP. TvZ is the guarantor for this work.

AUTHOR CONTRIBUTIONS

Conceptualization: TvZ; Data Curation: TvZ, EL, LAS; Formal Analysis: EL, LAS, EF, TvZ; Funding Acquisition: SP, TvZ; Investigation: EL, LAS, EF; Methodology: LAS, EL, EF; Project Administration: SM, SP, TvZ; Resources: LAS, EL, EF; Supervision: SP, SM, TvZ; Validation: EL, LAS, TvZ; Visualization: EL, LAS, EF, TvZ; Writing - Original Draft Preparation: TvZ; Writing - Review and Editing: EL, LAS, SM, EF, SP, TvZ

Disclaimer

The sponsors had no role in study design; collection, analysis, and interpretation of data; writing of the report; and decision to submit the article for publication.

***Evon Low*[1,4], *Lucy A. Smith*[2,4], *Satomi Miwa*[1], *Edward Fielder*[1], *Stefan Przyborski*[2,3,*] *and Thomas von Zglinicki*[1,*]**

[1]*Biosciences Institute, Faculty of Medical Sciences, Newcastle University, Newcastle upon Tyne, United Kingdom;* [2]*Department of Biosciences, Durham University, Durham, United Kingdom; and* [3]*Reprocell Europe Limited, Thomson Pavilion, Glasgow, United Kingdom*

[4]*These authors contributed equally to this work.*

[*]*Corresponding author e-mails: stefan.przyborski@durham.ac.uk and t.vonzglinicki@ncl.ac.uk*

SUPPLEMENTARY MATERIAL

Supplementary material is linked to the online version of the paper at www.jidonline.org, and at https://doi.org/10.1016/j.jid.2024.07.004.

REFERENCES

Blokland KEC, Pouwels SD, Schuliga M, Knight DA, Burgess JK. Regulation of cellular senescence by extracellular matrix during chronic fibrotic diseases. Clin Sci (Lond) 2020;134:2681–706.

Costello L, Fullard N, Roger M, Bradbury S, Dicolandrea T, Isfort R, et al. Engineering a multilayered skin equivalent: the importance of endogenous extracellular matrix maturation to provide robustness and reproducibility. Methods Mol Biol 2019;1993:107–22.

Diekmann J, Alili L, Scholz O, Giesen M, Holtkötter O, Brenneisen P. A three-dimensional skin equivalent reflecting some aspects of in vivo aged skin. Exp Dermatol 2016;25:56–61.

Janson D, Rietveld M, Willemze R, El Ghalbzouri A. Effects of serially passaged fibroblasts on dermal and epidermal morphogenesis in human skin equivalents. Biogerontology 2013;14:131–40.

Kirkland JL, Tchkonia T. Cellular senescence: a translational perspective. EBioMedicine 2017;21:21–8.

Low E, Alimohammadiha G, Smith LA, Costello LF, Przyborski SA, von Zglinicki T, et al. How good is the evidence that cellular senescence causes skin ageing? Ageing Res Rev 2021;71:101456.

Mavrogonatou E, Papadopoulou A, Pratsinis H, Kletsas D. Senescence-associated alterations in the extracellular matrix: deciphering their role in the regulation of cellular function. Am J Physiol Cell Physiol 2023;325:C633–47.

Roger M, Fullard N, Costello L, Bradbury S, Markiewicz E, O'Reilly S, et al. Bioengineering the microanatomy of human skin. J Anat 2019;234:438–55.

Weinmüllner R, Zbiral B, Becirovic A, Stelzer EM, Nagelreiter F, Schosserer M, et al. Organotypic human skin culture models constructed with senescent fibroblasts show hallmarks of skin aging. NPJ Aging Mech Dis 2020;6:4.

SUPPLEMENTARY MATERIALS AND METHODS

Primary cells and cell maintenance

Neonatal human dermal fibroblasts were cultured in either DMEM, supplemented with 5 ml of L-glutamine (G7513-100ML), 5 ml penicillin/streptomycin, and 50 ml foetal bovine serum (Sigma, F9665-500ML) or Human Fibroblast Expansion Basal Medium (Fisher Scientific UK, M106500) supplemented with Low Serum Growth Supplement (Fisher Scientific UK, S00310) and gentamicin (Fisher Scientific, G418 Sulfate) at a 37 °C humidified atmosphere with 5% carbon dioxide. Cells were bought from Life Technologies, Thermo Fisher Scientific in 2017 (lot number 1366434) and were regularly validated (by morphology and onset of replicative senescence at population doubling ≅50) and mycoplasm tested (bimonthly).

Neonatal human epidermal keratinocytes were cultured in Epilife Medium with 60 μM calcium (Fisher Scientific UK, MEPI500CA) supplemented with Human Keratinocyte Growth Supplement (Fisher Scientific UK, S0015) and gentamicin (Fisher Scientific, G418 Sulfate) at a 37 °C humidified atmosphere with 5% carbon dioxide. Cells were bought from Life Technologies, Thermo Fisher Scientific in 2021 (lot number 2018512) and were bimonthly tested for mycoplasms.

Induction of cellular senescence

To induce cellular senescence, fibroblasts were subjected to 20 Gy ionising X ray radiation. Cells were then maintained for at least 10 days to allow a fully senescent phenotype to develop (Passos et al, 2010). Cell numbers remained constant for at least 30 days after irradiation. The senescent phenotype was confirmed by absence of Ki-67 staining, low levels of HMGB1 and laminB1, and increased nuclear size (Supplementary Figure S1).

Skin equivalent generation

Full-thickness human skin equivalents were generated using Alvetex technology as described in Roger et al (2019), with minor protocol modifications to incorporate senescent cells into the dermal compartment.

To generate dermal equivalents containing senescent fibroblasts, neonatal and senescent fibroblasts were combined at various ratios and seeded onto Alvetex scaffolds, with the final number of cells seeded kept consistent according to the size of the Alvetex insert (0.5 M total cells for 12-well inserts, 0.17 M total cells for 24-well inserts). After seeding, all dermal models were maintained as described in Roger et al (2019) for 28 days, at which point human epidermal keratinocytes were seeded onto the constructs to form full-thickness skin models. These were maintained for 14 days at the air−liquid interface before harvesting for downstream analysis.

Processing

Full-thickness human skin equivalents were unclipped from the inserts, rinsed with PBS, and fixed in 4% paraformaldehyde for 2 hours at room temperature. The models were then dehydrated in a graded ethanol series for 15 minutes each (30, 50, 70, 80, 90, 95, and 100%). Models were transferred to plastic cassettes and immersed in Histoclear for 30 minutes, followed by a mixture of Histoclear and melted wax (1:1 ratio) for at least 30 minutes in the 60 °C oven. Then, models were moved to full melted wax for 60 minutes before being fully embedded in wax in moulds.

H&E staining

Slides were deparaffinized and hydrated through a series of ethanol before washing in distilled water. Slides were incubated in Mayer's Hematoxylin (Sigma-Aldrich) for 5 minutes, before washing for 30 seconds in distilled water. Slides were then dehydrated in 70% ethanol for 30 seconds before incubating in alkaline alcohol for 30 seconds to blue the nuclei. Slides were further dehydrated in 95% ethanol before incubation in eosin for 30 seconds. Slides were finally washed in 95% ethanol before further dehydration and clearing in 100% ethanol and Histoclear. Slides were mounted onto glass coverslips using Histomount and imaged using a Nikon E800 microscope at ×200 magnification.

Immunostaining

After deparaffinization, antigen retrieval, and washing, samples were incubated in blocking solution—1:60 (normal goat serum):(0.1% BSA/PBS) or 1:4 (normal calf serum):(0.4% Triton/PBS)—for 1 hour at room temperature, followed by incubation with primary antibody overnight at 4 °C (Supplementary Table S3). The samples were washed in PBS 3 times for 5 minutes each, followed by an hour of secondary antibody incubation at room temperature. Samples were mounted onto microscope slides with VECTASHIELD Antifade Mounting Medium with DAPI (H-1200-10).

Collagen assay

The total collagen content in punch biopsies was measured by the QuickZyme Total Collagen Assay (QuickZyme Biosciences) according to the manufacturer's instructions. Punch biopsies were used to standardize the area when the samples were taken. The assay measures total collagen content in μg/ml, so the values were normalized to the control value for each experiment to enable comparison (and account for variation between experiments).

Secreted proteins in the supernatant

Media samples were collected at the end of culture by removing 1 ml media from each well/plate and storing at −80 °C. Samples were shipped frozen to Eve Technologies (Calgary, Canada) for selected cytokine arrays to be performed: Human Cytokine Proinflammatory Focused 15-Plex Discovery Assay Array (human dermal fibroblast 15) and human matrix metalloproteinase and tissue inhibitor of metalloproteinase Discovery Assay Array for cell culture and nonblood samples (human matrix metalloproteinase/tissue inhibitor of metalloproteinase-C,O).

Technical repeats and operationalization of measurements

Embedded samples were divided in 2 and separately processed and analyzed in independent laboratories. Laboratory/observer B was fully blinded to the senescent fibroblast density in the model. Pilot experiments showed a high degree of variation between estimates by independent observers. Therefore, observers agreed on the following operationalizations before the actual experiments:

1. Epidermal thickness was measured on H&E-stained sections. A grid was

overlaid onto the images at regular 50 μm intervals, and the epidermal thickness was measured using the straight-line tool in ImageJ. A total of 300 measurements were made across the entire length of the model, avoiding only areas that showed embedding artefacts, measured from the bottom of the basal cells to the bottom of the stratum corneum as exemplified in Supplementary Figure S7.

2. Basal cell and nuclear size were measured on anti-cytokeratins 10/14–stained immunofluorescence images. To be included, cells had to touch the basal membrane and be completely identifiable and nonoverlapping. A total of 300 cells per sample were measured using the circumference tool in ImageJ.
3. Immunofluorescence. After finding significant inter and intraobserver variation when positive cells were manually identified, nuclei were identified as positive when their mean fluorescence values (mean gray value, measured in ImageJ) was greater than average background plus 2 SD. Average background was calculated separately for each image from 5 clearly negative cells. About 300 cells per experimental condition were measured on 5–7 images. Fractions of positive cells were expressed as percentage of all cells in the respective (basal or suprabasal) layer.

Statistics

To show effects of both interexperimental and technical variation, data were presented as superplots (Lord et al, 2020). The effects of variable seeding densities of senescent dermal fibroblasts were assessed by linear regression. For quantitative size measurement (epidermal thickness, basal cell and nuclear area) averages per condition, experiment and laboratories were used as individual data points, whereas for cell fractions estimated by immunofluorescence, averages per image represented the individual data entries. To assess interlaboratory variability, 2-way ANOVA was carried out on both raw and normalized datasets.

SUPPLEMENTARY REFERENCES

Lord SJ, Velle KB, Mullins RD, Fritz-Laylin LK. SuperPlots: communicating reproducibility and variability in cell biology. J Cell Biol 2020;219:e202001064.

Passos JF, Nelson G, Wang C, Richter T, Simillion C, Proctor CJ, et al. Feedback between p21 and reactive oxygen production is necessary for cell senescence. Mol Syst Biol 2010;6:347.

Roger M, Fullard N, Costello L, Bradbury S, Markiewicz E, O'Reilly S, et al. Bioengineering the microanatomy of human skin. J Anat 2019;234:438–55.

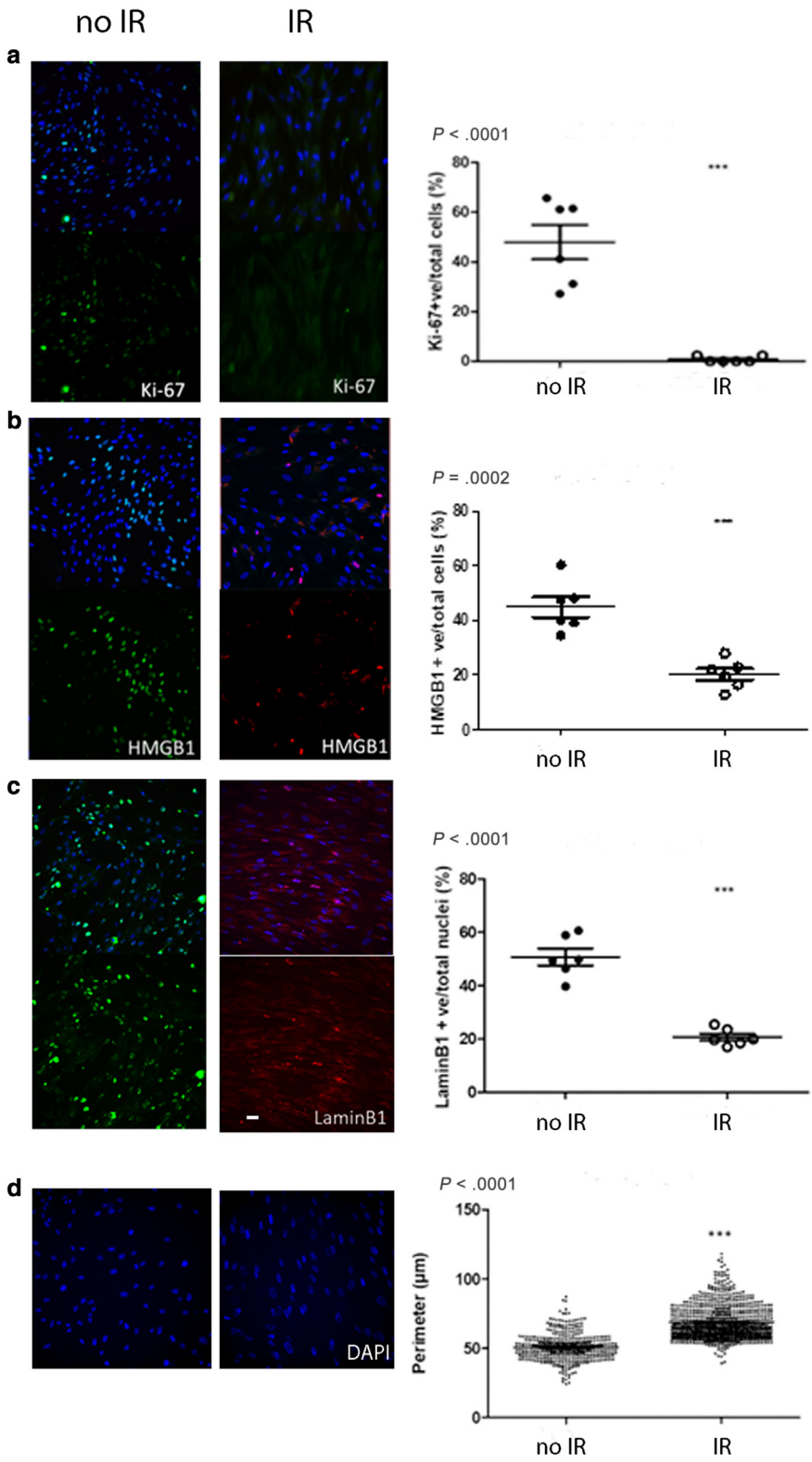

Supplementary Figure S1. Senescence markers in irradiated HDFs. Low PD neonatal HDFs were irradiated with 20 Gy and kept for 10 days before processing for IR. Nonirradiated HDFs were used as controls (no IR). Data are means ± SEM of 6 images per condition (for **a**–**c**) or all nuclei measured on 6 images (for **d**). Magnification bar = 20 mm. HDF, human dermal fibroblast; IR, ionising radiation; PD, population doubling.

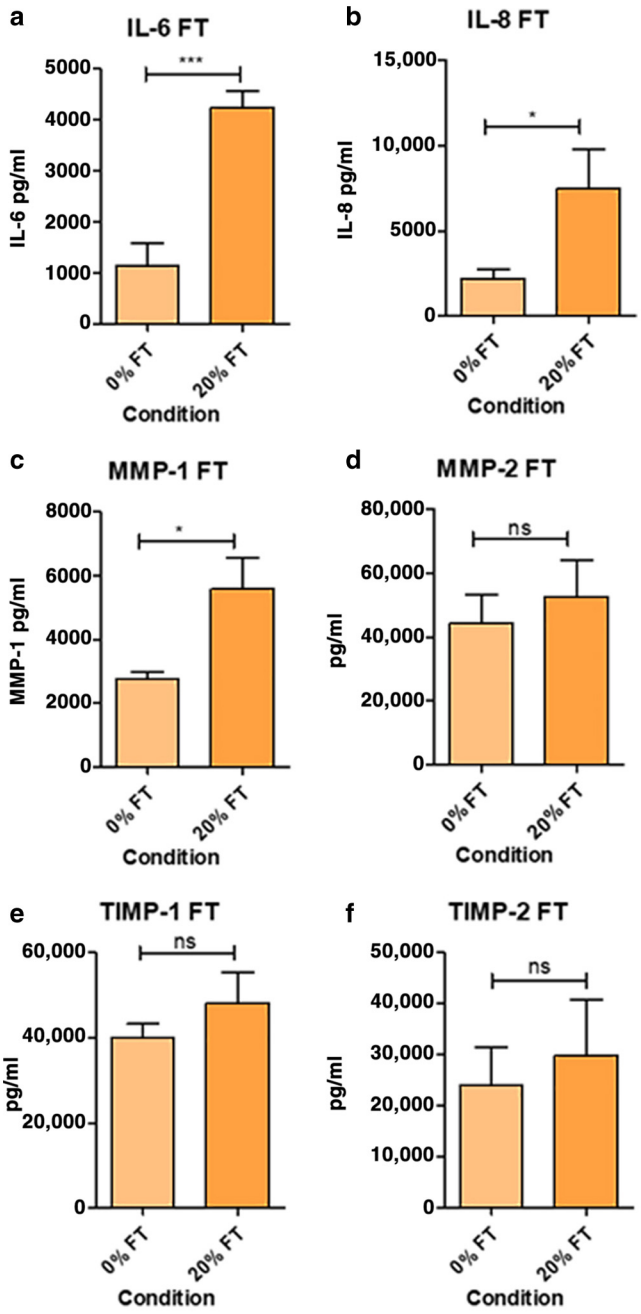

Supplementary Figure S2. Concentrations of SASP components in the supernatant of 3-dimensional full-thickness skin equivalents generated with no or 20% senescent HDFs as measured by cytokine array. Supernatants were taken at the end of culture. (**a**) IL-6, (**b**) IL-8, (**c**) MMP1, (**d**) MMP2, (**e**) TIMP1, and (**f**) TIMP2. Data are mean ± SEM, with n = 3 independent experiments. ***$P < .001$, **$P < .01$, and *$P < .05$, ns indicates $P > .05$. FT, full thickness; HDF, human dermal fibroblast; MMP, matrix metalloproteinase; ns, not significant; SASP, senescence-associated secretory phenotype; TIMP, tissue inhibitor of metalloproteinase.

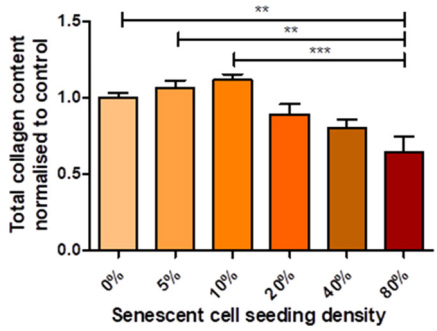

Supplementary Figure S3. Total collagen content in the dermal equivalent in 3-dimensional skin models measured using the QuickZyme Total Collagen assay. Data are normalized to the control models. Data are presented as mean ± SEM, with n ≥ 3 models per condition. ***$P < .001$ and **$P < .01$, with 1-way ANOVA. Regression analysis results in a negative slope of −0.0051 ± 0.001 (mean ± SD). $P < .001$.

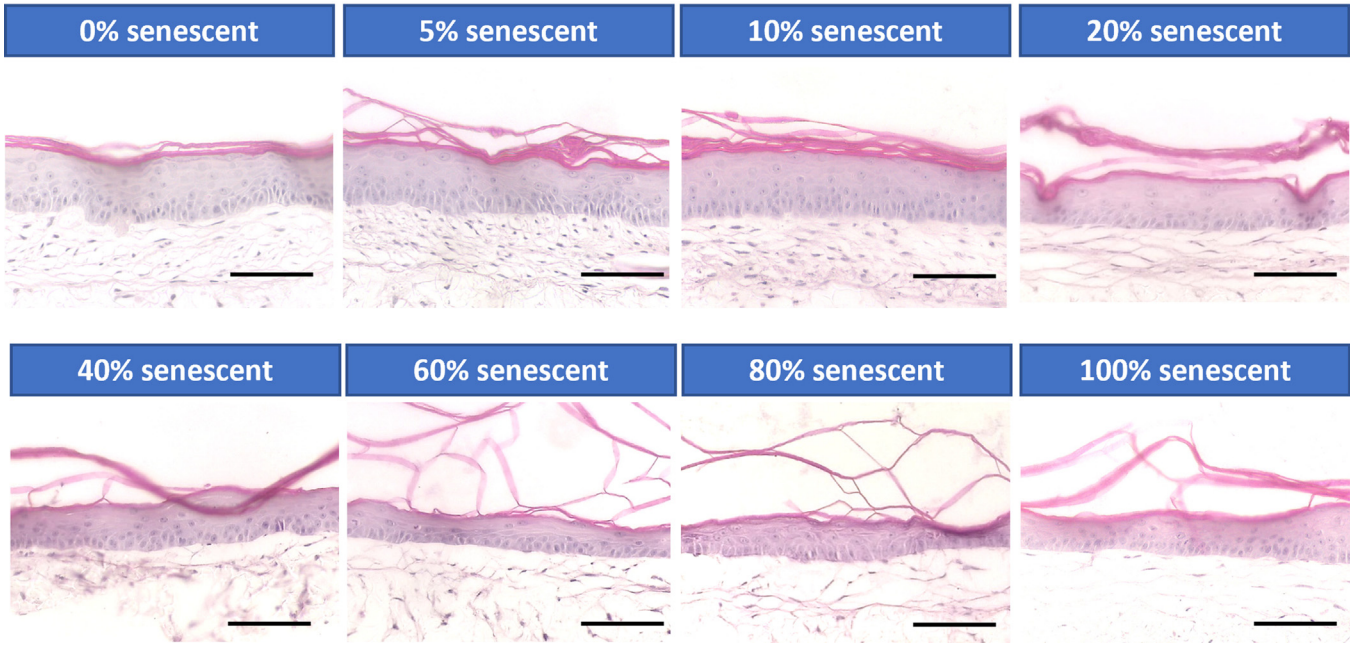

Supplementary Figure S4. H&E images of full-thickness 3-dimensional skin models. Senescent cell seeding densities are indicated on top of the micrographs. Magnification bar = 100 mm.

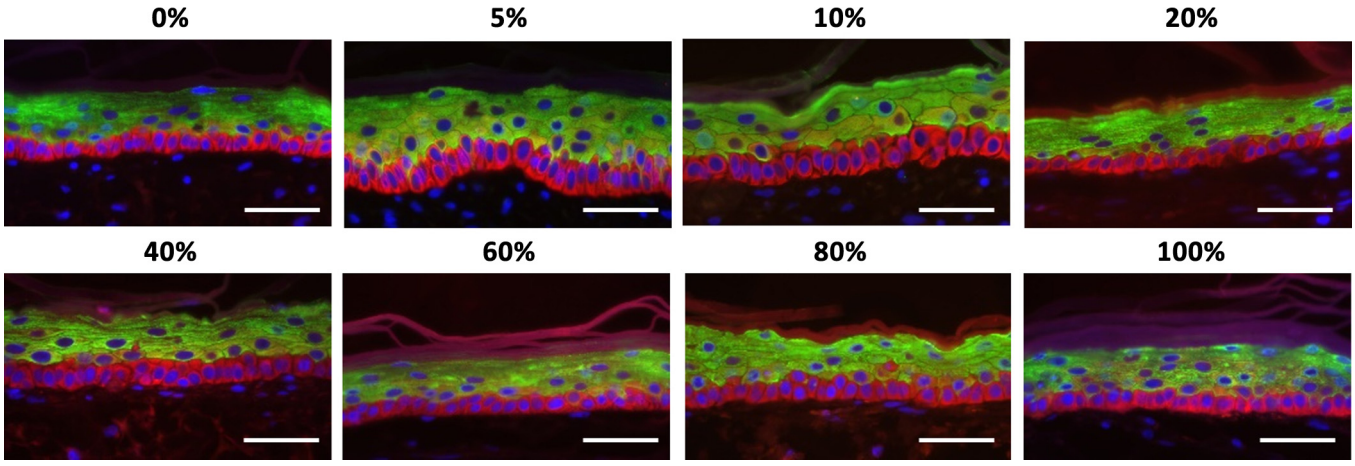

Supplementary Figure S5. K10/K14 micrographs of full-thickness 3-dimensional skin models. Senescent cell seeding densities are indicated on top of the micrographs. Magnification bar = 50 mm. red: K14, green: K10, and blue: Hoechst. K10, keratin 10; K14, keratin 14.

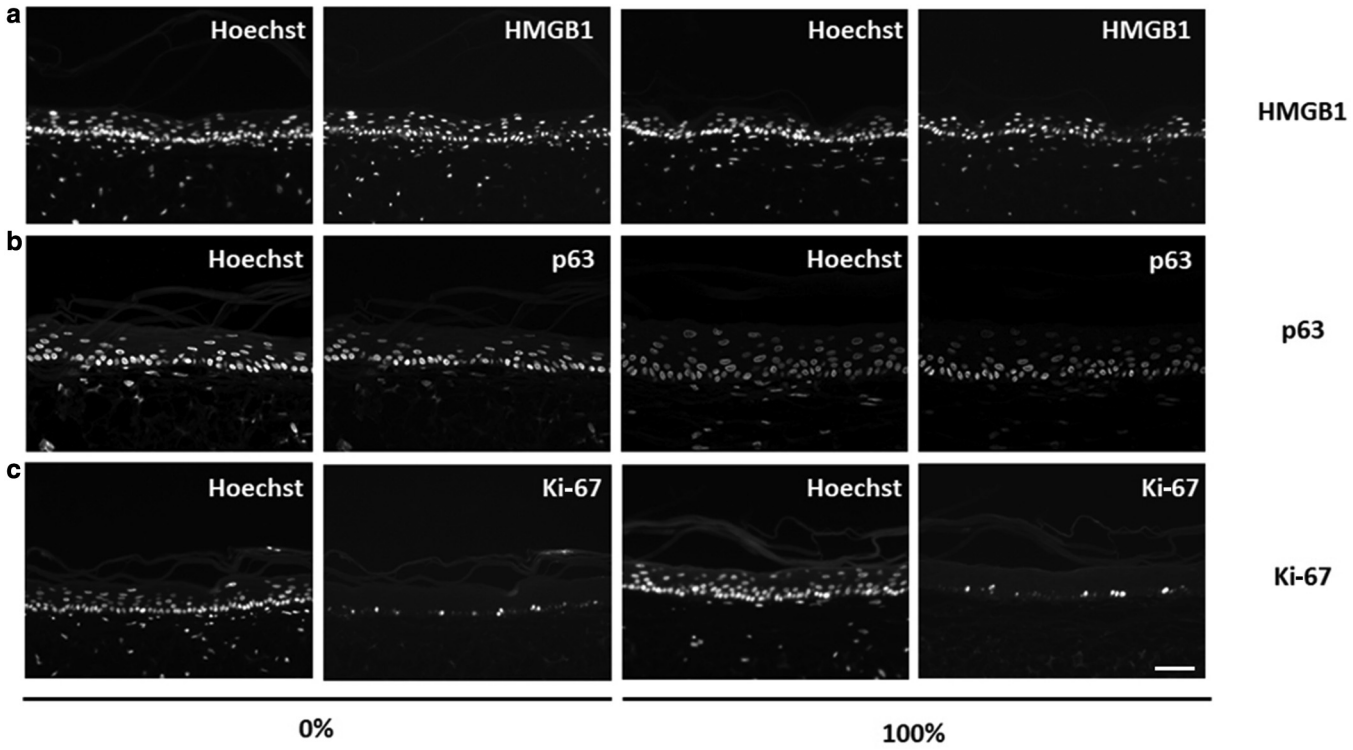

Supplementary FigureS6. Representative immunofluorescence micrographs of full-thickness models with either 0 or 100% senescent cell seeding density for HMGB1, p63, and Ki-67. (**a**) HMGB1, (**b**) p63, and (**c**) Ki-67. Magnification bar = 50 mm.

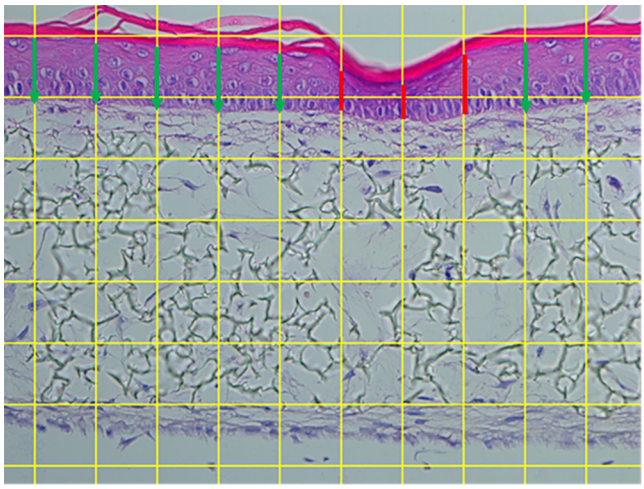

Supplementary Figure S7. Principle of epidermal thickness measurements. Green arrows denote measurement included. Red bars denote excluded (embedding artefact due to dehydration).

Supplementary Table S1. Two-Way ANOVA *P*-Values on Raw Data

Parameter	p Lab A versus B	p Senescence
Epidermal thickness	.8966	.6892
Basal cell size	.0373	.7557
Basal cell nuclear size	.0043	.7881
HMGB1 basal	<.0001	.0853
HMGB1 suprabasal	.0568	.8144
Ki-67 basal	.0028	.5608
p63 basal	.3182	.2073

P-values indicate differences between laboratories (p Lab A vs B) and between senescent fibroblast seeding densities (p Senescence). Interaction *P*-values were all nonsignificant.

Supplementary Table S2. Two-Way ANOVA *P*-Values for Normalized Data

Parameter	p Lab A versus B	p Senescence
Epidermal thickness	.4786	.8509
Basal cell size	.0271	.0016
Basal cell nuclear size	.2387	.0981
HMGB1 basal	.9705	.7462
HMGB1 suprabasal	.1336	.8415
Ki-67 basal	.9725	.7470
p63 basal	.2747	.0030

P-values indicate differences between laboratories (p Lab A vs B) and between senescent fibroblast seeding densities (p Senescence). Interaction *P*-values were all nonsignificant.

Supplementary Table S3. Antibodies for Immunostaining

Primary Antibody	Dilution	Provider	Host	Catalog Number	Secondary Antibody	Dilution	Mounting
Ki-67	1:250	Abcam	Rabbit	Ab15580	Alexa Fluor 488 goat anti rabbit	1:1000	VECTASHIELD Antifade Mounting Medium with DAPI (H-1200-10).
LaminB1	1:250 (cells) 1:200 (tissue)	Abcam	Rabbit	Ab16048	Alexa Fluor 488 goat anti rabbit	1:1000	
HMGB1	1:250 (cells) 1:200 (tissue)	Abcam	Rabbit	Ab79823	Alexa Fluor 488 goat anti rabbit	1:1000	
P63	1:250	Abcam	Rabbit	Ab124762	Alexa Fluor 488 goat anti rabbit	1:1000	
Cytokeratin 14	1:200	Abcam	Mouse	Ab7800	Alexa Fluor 488 goat anti mouse	1:1000	
Cytokeratin 10	1:250	Abcam	Rabbit	Ab766318	Alexa Fluor 594 goat anti rabbit	1:1000	
acGFP	1:100	Takara	Rabbit	632592	Alexa Fluor 488 goat anti mouse	1:1000	